Catalysis Today 153 (2010) 162–169

Contents lists available at ScienceDirect

Catalysis Today

journal homepage: www.elsevier.com/locate/cattod

Research on assembly of nano-Pd colloid and fabrication of supported Pd catalysts from the metal colloid

Licheng Liu, Ting Wei, Xuehong Zi, Hong He*, Hongxing Dai

Department of Chemistry and Chemical Engineering, College of Environmental and Energy Engineering, Beijing University of Technology, Beijing 100124, China

ARTICLE INFO

Article history:
Available online 7 May 2010

Keywords:
Pd nanoparticles
Orthogonal experiment
Colloid
Pd catalyst
CO oxidation

ABSTRACT

The ultrasonic-assisted membrane reduction (UAMR) method was used to prepare colloidal Pd nanoparticles. An orthogonal experiment was performed to investigate the effect of synthesis parameters in UAMR on Pd particle size. The average Pd particle size can be regulated in a wide range of 5–220 nm. The fabrication of supported Pd catalyst from a typical nano-sized Pd colloid with 1 wt% Pd loading was studied. The colloid and as-prepared catalyst were characterized by TEM, BET, ICP-OES, XRD, H_2-TPR, and CO catalytic oxidation. Fabrication methods would have significant impacts on the actual Pd content, metal dispersion, PdO/Pd reducibility, textural property, etc., over different supports. The CO oxidation activity of the catalysts was consequently decided by these characters. The Pd/$Ce_{0.5}Zr_{0.5}O_2$ catalyst prepared by adsorbing Pd nanoparticles on $Ce_{0.5}Zr_{0.5}O_2$ showed the highest activity with CO complete oxidation at 150 °C among all of the catalysts investigated.

1. Introduction

As we all know, three-way catalysts (TWCs) have been successfully applied in automobile emissions control. Generally, TWCs comprised of ceramic monolith carrier, γ-Al_2O_3-based washcoat, and Pt, Pd, Rh precious metals as active components [1,2]. There are still some challenges remained about TWCs for the future application: (i) to improve the catalytic activity, especially at relative low temperature; (ii) to reduce the amount of precious metals in TWCs; (iii) to eliminate NO_x at lean burn conditions [3,4]. The former two aspects are related to the valid usage of the precious metals.

The activity of transition metal catalyst is determined by many factors, such as the metal loading, composition, chemical state (oxidized or reduced), and metal dispersion [5,6]. In the view of nano-scale, the activities of precious metals depend on the nanoparticle size, morphology, exposed crystal facets, surface assembly, etc. Many researchers have studied the size or shape dependence of metal nanoparticles on activity and selectivity in catalytic reaction [7–11]. Goodman found that the highest activity of CO oxidation could be obtained over Au/TiO_2(1 1 0) catalyst with the supported Au particles in the size of ca. 3 nm. Both of smaller and bigger Au particles would result in a decrease in activity under the given reaction condition [7]. Somorjai and his coworkers investigated the benzene hydrogenation over the Pt nanocrystals with the cube and cuboctahedral morphology, respectively. The results showed that both of cyclohexane and cyclohexene could be produced over cuboctahedral Pt nanocrystals, whereas only cyclohexane was produced on cube Pt nanocrystals [8,9].

During the past decade, many attempts have been devoted to the research on controllable fabrication of colloidal metal and alloy nanoparticles with desirable size and shape as well as some valuable results were obtained [12,13]. The nano-sized metal colloids can be used as catalysts directly for some liquid organic reactions [14]. It is meaningful if supported metal catalysts, which are widely used in the modern chemical industry, could be fabricated from nano-sized metal colloids. The key issue is how to remove the surfactant stabilizer. Precipitation and rinsing are optional for the preparation. Solvent evaporation or particles adsorption on the surface of carriers is also the alternative based on the solvent or carrier properties [15].

The fabrication of nano-sized colloidal metals with the desirable size and shape is the important step in the novel process of catalyst preparation. Many methods have been developed to controllable synthesis of metal nanoparticles [12,13]. Recently, we reported a method, i.e. ultrasonic-assisted membrane reduction (UAMR), for fabrication of colloidal Ag and Au nanocrystals [16]. In this paper, the synthesis of Pd colloids by UAMR method was reported. The effects of synthesis parameters on the particle size were investigated by performing an orthogonal experiment. Several carriers (Al_2O_3, TiO_2, SiO_2, CeO_2, $Ce_{0.5}Zr_{0.5}O_2$) were employed in the preparation of supported Pd catalysts with a nano-Pd colloid. The catalytic activities of the prepared catalysts, especially

* Corresponding author at: Laboratory of Catalysis Chemistry and Nanoscience, Department of Chemistry and Chemical Engineering, Beijing University of Technology, No. 100 Pingleyuan, Chaoyang District, Beijing 100124, China.
Fax: +86 10 67396588.
E-mail address: hehong@bjut.edu.cn (H. He).

0920-5861/$ – see front matter © 2010 Elsevier B.V. All rights reserved.
doi:10.1016/j.cattod.2010.04.003

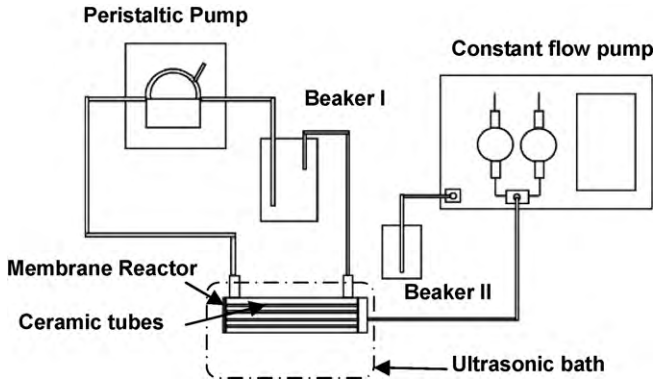

Scheme 1. Schematic of ultrasound-assisted membrane reduction (UAMR) device for the synthesis of metal nanocrystals.

Table 1
The factor-level table used in the orthogonal experiment for Pd nanoparticle synthesis by UAMR method.

Level	Factor						
	A (ml/min)	*B* (ml/min)	*C* (mmol/L)	*D*	*E*	*F* (Hz)	*G* (nm)
1	1	100	40	5:1	1:1	0	40
2	5	300	80	15:1	10:1	50	100
3	10	600	200	30:1	20:1	100	200

A, reductant ($NaBH_4$) injection rate; *B*, Pd precursor solution circulating rate; *C*, $Pd(NO_3)_2$ concentration; *D*, $NaBH_4$ concentration (expressed as $NaBH_4$/Pd mass ratio); *E*, stabilizer (PVP) concentration (expressed as PVP/Pd molar ratio); *F*, ultrasonic frequency; *G*, hole size in membrane tube.

the Pd/Al_2O_3 and $Pd/Ce_{0.5}Zr_{0.5}O_2$ catalysts prepared by different processes, were evaluated.

2. Experimental

2.1. Assembly of nano-Pd colloid by UAMR

The schematic diagram of UAMR method is presented in Scheme 1. In a typical synthesis, the calculated amount of Pd precursor salts ($Pd(NO_3)_2$) and stabilizer of PVP were dissolved in D.I. water to give an aqueous solution (loaded in Beaker I) under vigorous stirring. The precursor solution was driven by a peristaltic pump to form a cycling flow. A reductant solution (in Beaker II) prepared by dissolving a desired amount of $NaBH_4$ in D.I. water was injected into the membrane reactor by a constant flowing pump. The reactor was composed of three ceramic membrane tubes with a canular glass tube outside. The Pd precursor solution flowed in the glass tube reactor and outside ceramic tubes. The $NaBH_4$ solution was forced into the ceramic tubes and infiltrated through the abundant holes on the wall of the ceramic tubes into the glass tube reactor, in where, the reduction of Pd^{2+} ions by $NaBH_4$ occurred immediately when the two solutions encountered. The synthesis process was stopped after complete consumption of the $NaBH_4$ solution. The membrane reactor was kept in an ultrasonic bath to strengthen the dispersion and mass transfer for the reactants.

2.2. Orthogonal experiment on Pd nanoparticles synthesis

In the synthesis of Pd nanoparticles by UAMR method, there are several factors that can be regulated. By adjusting these factors, a seven three-level factors orthogonal experiment was carried out according to an $L_{27}(3^{13})$ orthogonal table. The Pd nanoparticle size was measured by a laser particle size analyzer (PSS Nicomp 380 ZLS). The factor-level table was shown in Table 1.

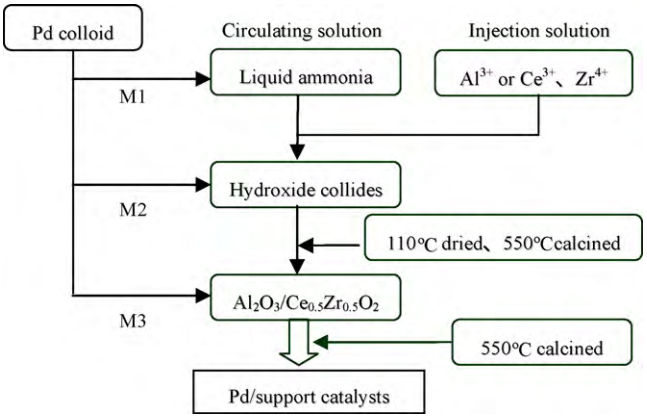

Scheme 2. Illustration of Pd/Al_2O_3 and $Pd/Ce_{0.5}Zr_{0.5}O_2$ catalysts combined with the preparation of Al_2O_3 and $Ce_{0.5}Zr_{0.5}O_2$ support.

2.3. The synthesis of nano-sized Pd colloid used to prepare the supported Pd catalysts

The Pd colloid used for catalyst preparation was synthesized according to the following conditions: the circulating velocity = 400 ml/min, injection velocity = 1 ml/min, $Pd(NO_3)_2$ precursor = 80 mmol/L, $NaBH_4$/Pd (mass ratio) = 10/1, PVP/Pd (molar ratio) = 20/1, ultrasonic frequency = 24 kHz, hole size on the wall of membrane tube = 40 nm.

2.4. The fabrication of supported Pd catalysts by UAMR from nano-sized Pd colloid

The Pd/supports (support = Al_2O_3, TiO_2, SiO_2, CeO_2, $Ce_{0.5}Zr_{0.5}O_2$) catalysts were fabricated by the UAMR method. In the process, a suitable amount of support powder was put into the Pd colloid on the basis of 1.0 wt% Pd loading. The mixture was filtrated and washed after stirring for 24 h at room temperature. The resulted solid was dried at 60 °C and calcined at 550 °C for 3 h, giving the Pd/Al_2O_3, Pd/TiO_2, Pd/SiO_2, Pd/CeO_2, and $Pd/Ce_{0.5}Zr_{0.5}O_2$ catalysts. The Al_2O_3, TiO_2 and SiO_2 were purchased from Zhejiang Ultrafine Powder & Chemicals CO. Ltd., whereas the CeO_2 and $Ce_{0.5}Zr_{0.5}O_2$ were prepared by the same UAMR method.

The conventional impregnation method was also applied for the synthesis of Pd supported on different carriers such as Al_2O_3, SiO_2, TiO_2, and $Ce_{0.5}Zr_{0.5}O_2$ using $Pd(NO_3)_2$ precursor. The Pd loading was still 1.0 wt%. The drying and calcination were the same to above process.

2.5. The fabrication of Pd/Al_2O_3 and $Pd/Ce_{0.5}Zr_{0.5}O_2$ by UAMR combined with support preparation

The Pd/Al_2O_3 and $Pd/Ce_{0.5}Zr_{0.5}O_2$ catalysts were also prepared according to the processes illustrated in Scheme 2, which were indicated as M1, M2 and M3. The precipitant ($NH_3{\cdot}H_2O$) was placed in Beaker I as circulating solution and Al^{3+} or Ce^{3+} and Zr^{4+} ions solution was placed in Beaker II and injected to the membrane reactor. For M1 sample, the Pd colloid was added to the liquid ammonia as circulating solution. The co-precipitation occurred in the UAMR reactor. The resulting solid was filtrated, washed, dried at 110 °C and calcined at 550 °C for 3 h to give M1 sample. For M2 sample, hydroxide colloid of Al_2O_3 or $Ce_{0.5}Zr_{0.5}O_2$ precursor was firstly prepared by the UAMR method and mixed with proper Pd colloid under stirring for 0.5 h. The solid mixture was then filtrated, washed, dried at 110 °C and calcined at 550 °C for 3 h to give M2 samples. For M3 sample, the Al_2O_3 or $Ce_{0.5}Zr_{0.5}O_2$ supports was firstly prepared by UAMR. The prepared support was put into Pd colloid to fabricate M3

catalysts, which was identical to the procedure of other supported Pd catalysts.

2.6. Characterization

The Pd nanoparticles were characterized by a Transmission Electron Microscope (JEM-2010) operating at 200 kV. The metal colloid was deposited on a carbon coating copper grid before TEM examination after pretreatment under ultrasonic for 15 min.

Hydrogen temperature-programmed reduction (H_2-TPR) experiments were conducted with a sample (0.2 g) pretreated in situ in O_2/N_2 (20%, flow rate = 30 ml/min) at 500 °C for 1 h over a chemical adsorption apparatus (Micromeritics, AutoChem 2920 II). After cooling to RT in the same atmosphere, the sample was exposed to a flow (50 ml/min) of 10% H_2–90% Ar (v/v) and heated at a rate of 10 °C/min to 800 °C. The outlet gases were cooled by the mixture of isopropanol and liquid nitrogen to remove the water and analyzed online by a TCD detector. The H_2 consumption (μmol/g catalyst) was calculated based on reduction peak area, which was calibrated with a standard 0.02 g of CuO sample's H_2-TPR peak area for each sample.

X-ray diffraction (XRD) patterns of the catalysts were recorded on a X-ray diffractometer (Shimadzu XD-D1) operated at 40 kV and 20 mA using CuKa radiation and Ni filter. Diffraction peaks of crystal phases were referred to the database of 1998 ICDD PDF database for identification.

N_2 adsorption/desorption isotherms were determined on a physical adsorption apparatus (Micromeritics, ASAP 2020). The samples were pretreated at 300 °C under vacuum for 5 h before measurements. Calculations of the specific surface area (BET), pore volume, and average pore size (BJH method) were performed with the software of the apparatus.

The Pd content was analyzed by using an Inductively Coupled Plasma-Optical Emission Spectrometry (Perkin-Elmer, OPTIMA 5300DV). The known weight of catalyst was dissolved in the mixture of HCl and HNO_3 (3:1 proportion). After complete dissolution, the solution was diluted to required volume and analyzed for Pd content.

The metal dispersion was measured by O_2–H_2 titration on a chemical adsorption apparatus (Micromeritics, AutoChem 2920 II). The 0.2 g of catalyst was pretreated in 10% H_2/Ar at 350 °C for 60 min and 450 °C for 30 min and then purged in pure He (50 ml/min) at 450 °C for 60 min, then it was cooled to room temperature before the measurement. The catalyst was heated-up to 120 °C and treated for 30 min in a flow of 20% O_2/N_2. The pulse titration of pure H_2 began after sweeping for 30 min under Ar flow. The metal dispersion was calculated automatically with the software of the apparatus.

The catalytic performances of the catalysts for the CO oxidation were investigated in a fixed bed quartz reactor. Feed gas composition was 1% CO, 1% O_2 with He as balance at atmospheric pressure. The mass of catalyst loaded to the reactor was 0.05 g and total flow rate of the feed gas was maintained at 100 ml/min, which corresponding to a space velocity of 60,000 h^{-1}. The reactants and products were analyzed online with a gas chromatograph (Shimadzu GC-14C). The CO and O_2 were separated by a 5A molecular sieve packed column and analyzed by a TCD detector. Due to the low concentration of reactants and products in the gas flow, the volumetric change after reaction was ignored in calculation. The conversion of CO was calculated as follows:

$$X_{CO}(\%) = \left(1 - \frac{[CO]_{out}}{[CO]_{in}}\right) \times 100 \quad (1)$$

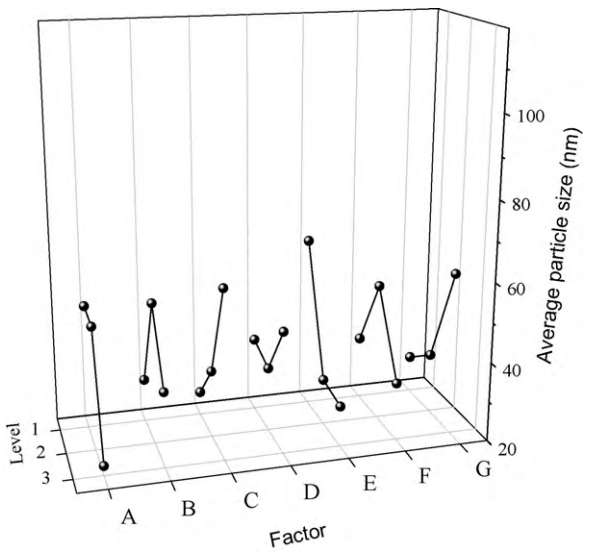

Fig. 1. Average particle size of Pd nanoparticle under three levels of 1, 2, 3 for each factor (the levels and factors can be referred to Table 1).

3. Results and discussions

3.1. Orthogonal experiment analysis

The average particle size of the nano-Pd in the experiment was in the range of 5.5–224 nm. The impact strength of different factors on the nanoparticle size was obtained by the range analysis on the experimental data. The capability of seven factors affecting the particle size was in the order of *C* ($Pd(NO_3)_2$ concentration) > *E* (PVP concentration) > *G* (hole size in membrane tube) > *A* ($NaBH_4$ injection rate) > *B* (Pd precursor solution circulating rate) > *F* (ultrasonic frequency) > *D* ($NaBH_4$ concentration). We also did analysis of variance of the experimental data. The *F*-distribution, which was used to check the significance of factor, suggested the same order of seven factors to impact on the Pd particle size. The concentrations of Pd^{2+} ions and PVP were the most two sensitive factors to influence Pd nanoparticle size.

The Pd particle size at three levels for each factor was plotted in Fig. 1. It can be seen that monotonic effect on particle size with the levels in the range was observed for some factors (*A*, *C*, *E*, and *G*). The increase of *A* ($NaBH_4$ injection rate) and *E* (PVP concentration)'s level resulted in a decrease of Pd particle diameter. The particle size increased with *C* ($Pd(NO_3)_2$ concentration) and *G* (hole size in membrane tube)'s level enhancement. The extreme value of particle size appeared as the three levels of *B* (Pd precursor solution circulating rate), *D* ($NaBH_4$ concentration) and *F* (ultrasonic frequency) factors were changed. So if we need to prepare small Pd nanoparticles by UAMR method, the following conditions can be considered: fast $NaBH_4$ injection rate, fast circulating rate (for reducing synthesis time), low Pd^{2+} concentration, $NaBH_4$/Pd (mass ratio) of 15, high PVP concentration, low ultrasonic frequency (for saving energy consumption), and small pore size on the wall of membrane tube.

3.2. Catalysts from nano-Pd colloid on different supports

The Pd colloid used for catalyst preparation, which was synthesized as described in Section 2, was characterized by TEM (Fig. 2). The size distribution of Pd nanoparticles was determined by measuring the diameter of 200 Pd particles in TEM image and presented also in Fig. 2. Spherical Pd nanoparticles with the size of smaller than 10 nm were observed and most of them were twinned par-

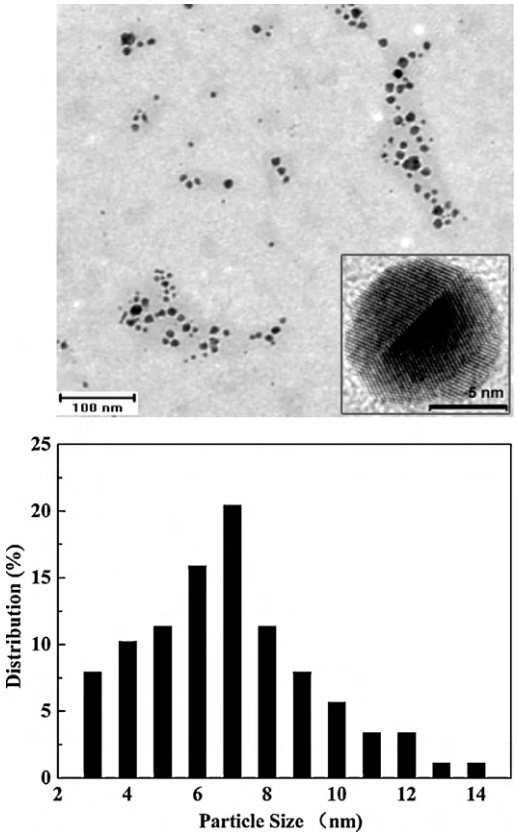

Fig. 2. TEM image of colloidal Pd nanoparticles and particle size distribution.

ticles (MTPs) [17]. The HRTEM image at the right low corner in the picture showed clear diffraction fringes and twinned crystal structure. The particle diameter was in the range of 3–14 nm and centered at 7 nm.

The powders of Al_2O_3, TiO_2, SiO_2, CeO_2, and $Ce_{0.5}Zr_{0.5}O_2$ were added to above Pd colloid, respectively, to prepare the catalysts with different supports and Pd loading of 1.0 wt%. Some physicochemical properties of the catalysts were summarized in Table 2. The catalysts showed significant differences in the textural properties (BET surface area, pore volume, and size) due to using the dissimilar supports. The CeO_2 and $Ce_{0.5}Zr_{0.5}O_2$ supported catalyst exhibited smaller pore volume and pore size than others. The Pd contents of catalysts were analyzed by ICP-OES, all of which were lower than the theoretical loading (1.0 wt%). In the catalyst preparation, the colloidal Pd nanoparticles interacted with support surface through electrostatic attraction, capillary adsorption, hydrogen bond, etc. So the properties of support, such as surface polarity and pore diameter, possessed significant effects on Pd nanoparticle adsorption and sediment, leading to the different actual Pd loadings. The textural property of catalyst was generally kept from that of the corresponding support. The small pore size and pore volume might limit the diffusion and ability of Pd colloid into the pores of CeO_2 and $Ce_{0.5}Zr_{0.5}O_2$, resulting in the low Pd loading for the Pd/CeO_2 and $Pd/Ce_{0.5}Zr_{0.5}O_2$ catalysts (both less than 0.3 wt%, Table 2). However, the high metal dispersion was obtained over the two catalysts. It was understandable that less Pd species would reduce aggregation.

The activities of the prepared catalysts for CO oxidation were presented in Fig. 3. The total CO conversion temperature ($T_{100\%}$) was in the temperature range of 150–250 °C. From Fig. 3, one can see that the activity of the catalyst decreased in the order of $Pd/Ce_{0.5}Zr_{0.5}O_2 > Pd/CeO_2 > Pd/Al_2O_3 > Pd/TiO_2 > Pd/SiO_2$. The light-off ($T_{50\%}$) temperatures were comparable to activity data

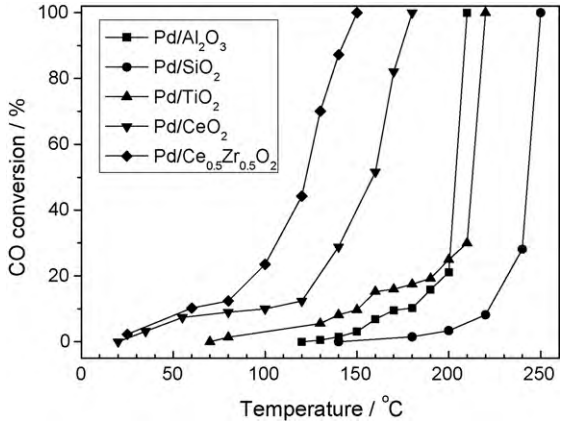

Fig. 3. CO conversion over Pd catalysts. Reaction conditions: 1% CO, 1% O_2, He balance; catalyst weight = 0.05 g, SV = 60,000 h^{-1}.

of Pd catalysts on different supports with 5 wt% Pd loading reported by Luo [18]. To our surprise, the Pd/CeO_2 and $Pd/Ce_{0.5}Zr_{0.5}O_2$ catalysts with actually very low Pd content in this study showed higher CO catalytic oxidation activity than other supported Pd catalysts. Many factors should be accounted for the activity differences, such as support properties, state of Pd (oxidized or reduced), and strong metal–support interaction (SMSI). But in present study, the number of exposed Pd species, which could provide active sites, might play an important role to dominate the catalytic activity. The exposed Pd species can be estimated by a multiply of actual Pd content with metal dispersion, higher values of which were gotten on Pd/CeO_2 and $Pd/Ce_{0.5}Zr_{0.5}O_2$ catalysts than on others.

For comparing the activity of the catalysts prepared by colloid sediment and conventional impregnation methods, the supported Pd catalysts with the Pd loading of 1.0 wt% were fabricated by impregnation method and the activities of the catalysts for CO oxidation were investigated under the same reaction conditions. Due to the difference of actual Pd content in catalysts, the CO oxidation activity was expressed as CO conversion rate ($\mu mol\ min^{-1}\ g^{-1}$). The napierian logarithm (Ln) of reaction rate was plotted with the reciprocal of absolute temperature to give the Arrhennius plot in Fig. 4, including Pd/Al_2O_3, Pd/TiO_2, Pd/SiO_2 and $Pd/Ce_{0.5}Zr_{0.5}O_2$ catalysts prepared by both UAMR and impregnation method. The apparent activation energy (E_a) can be calculated from the Arrhenius plot for each catalyst. The E_a of Pd/Al_2O_3, Pd/TiO_2, Pd/SiO_2, and $Pd/Ce_{0.5}Zr_{0.5}O_2$ catalysts prepared by UAMR were 71.8, 33.6, 92.2, and 12.5 kJ/mol, respectively. They were in accordance with the activities in Fig. 3, because low activation energy generally means high reaction rate constant. The catalysts prepared by impregnation exhibited E_a with higher values of 144.4, 37.2, 187.3 and 43.9 kJ/mol, respectively, than those of catalysts prepared by UAMR. These activation energies were comparable with those of Rh supported catalyst (~110 kJ/mol) reported by McClure and Goodman [19]. The catalysts prepared by UAMR method can markedly decrease the activation energy of CO oxidation, in comparison with catalysts prepared by conventional impregnation method.

3.3. Pd/Al_2O_3 and $Pd/Ce_{0.5}Zr_{0.5}O_2$ catalysts from nano-Pd colloid combined with support preparation

When the catalyst and support were prepared simultaneity in the nano-Pd colloid solution, the textural property of the prepared catalyst was changed. The XRD patterns of Pd/Al_2O_3 and $Pd/Ce_{0.5}Zr_{0.5}O_2$ catalysts fabricated with different processes (M1, M2 and M3 in Scheme 2) were shown in Fig. 5. In the XRD patterns of Pd/Al_2O_3 (Fig. 5a), the diffraction peaks corresponding to tetragonal γ-Al_2O_3 phase were seen at $2\theta = 37.4°$, 45.7°, 60.2° and

Table 2
Physico-chemical properties of Pd catalysts based on different supports.

Catalyst	BET surface area (m^2/g)	Pore volume (cm^3/g)	Pore size (nm)	Actual Pd (wt%)	Metal dispersion (%)
Pd/Al_2O_3	75.5	0.290	13.1	0.91	6.5
Pd/SiO_2	316.5	1.01	11.9	0.74	1.4
Pd/TiO_2	228.9	0.738	10.2	0.79	9.1
Pd/CeO_2	51.4	0.086	4.8	0.29	61.2
$Pd/Ce_{0.5}Zr_{0.5}O_2$	40.3	0.055	4.3	0.27	36.7

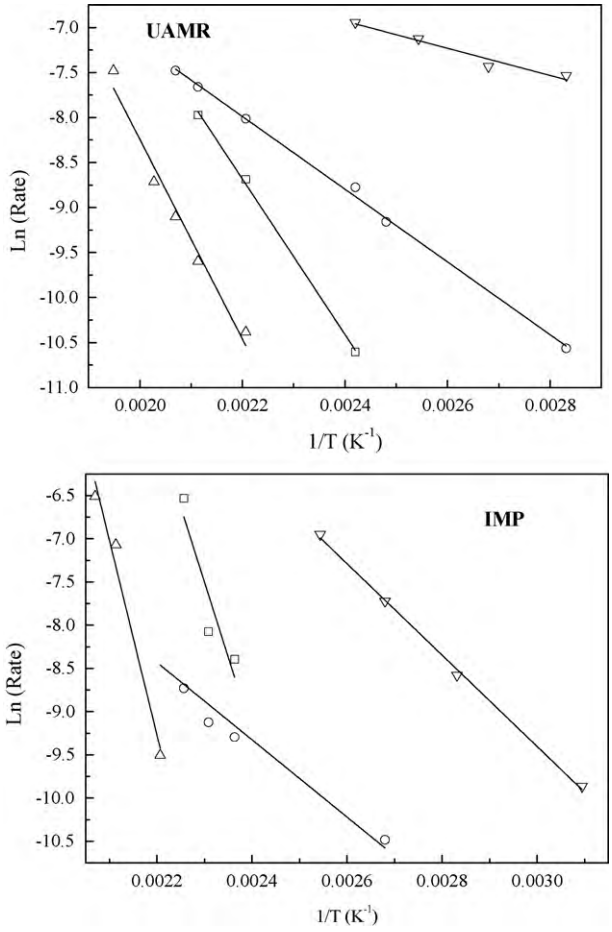

Fig. 4. Arrhenius plot of CO oxidation over Pd/Al_2O_3 (–□–), Pd/TiO_2 (–○–), Pd/SiO_2 (–△–), $Pd/Ce_{0.5}Zr_{0.5}O_2$ (–▽–) prepared by UAMR (up) and impregnation (down) method.

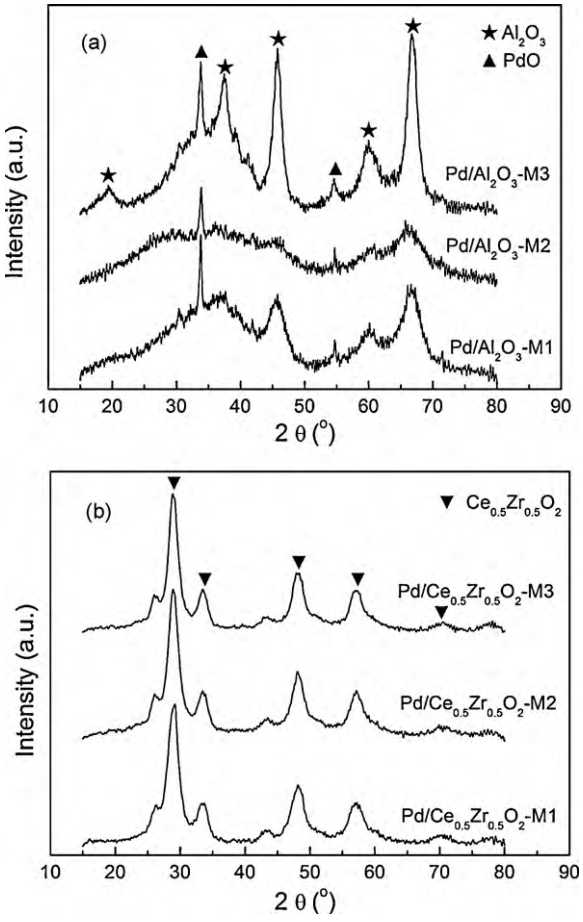

Fig. 5. XRD patterns of Pd/Al_2O_3 (a) and $Pd/Ce_{0.5}Zr_{0.5}O_2$ (b) catalyst.

66.7°. Peaks at 2θ value of 33.8° and 54.6° could be assigned to PdO. No Pd metal phase was detected [20–22]. The more intense peaks of Al_2O_3-M3 than others indicated that the Al_2O_3 support was the well crystallinity, which might be related to the calcinations of Pd/Al_2O_3-M3 two times. However, on the XRD patterns of $Ce_{0.5}Zr_{0.5}O_2$ (Fig. 5b), only peaks corresponding to cubic or tetrahedral (Ce, Ze)O phase (undistinguishable due to peak widening) were observed [23,24]. The diffraction peaks (2θ = 33.8°, 54.6°) induced by PdO or Pd were not differentiated due to overlap with diffraction peaks of $Ce_{0.5}Zr_{0.5}O_2$. Zhou et al. attributed the peak at 33.8° to PdO phase without exceptions when they studied $Pd/Ce_xZr_{1-x}O_2/SiO_2$ catalysts [25]. It is believed that the diffraction peak (2θ = 33.1°) of (2 0 0) facet of CeO_2 phase was omitted owning to the overlap.

The preparation of support (Al_2O_3 and $Ce_{0.5}Zr_{0.5}O_2$) in nano-Pd colloid (M1 in Scheme 2) created well textural structure due to the dispersion effect of the dissolved PVP polymer, which was approved by BET surface area and pore volume in Table 3. The Pd/Al_2O_3-M1 and $Pd/Ce_{0.5}Zr_{0.5}O_2$-M1 samples exhibited higher surface area and larger pore volume than another corresponding two samples (M2 and M3). The BET surface area, pore volume, and pore size of all Al_2O_3 based catalysts were larger than the corresponding $Ce_{0.5}Zr_{0.5}O_2$ based catalysts. The actual Pd content was different from each other but exhibited the same variety for the Pd/Al_2O_3 and $Pd/Ce_{0.5}Zr_{0.5}O_2$ catalysts. The Pd/Al_2O_3-M3 possessed lower actual Pd loading (0.44 wt%) than the Pd/Al_2O_3 prepared by supporting Pd on commercial Al_2O_3 (0.91 wt%), which was attributed to the different Al_2O_3 source (prepared by UAMR and commercial, respectively). Therefore, the variety and property of Al_2O_3 support plays an important role to determine the Pd loading when catalyst is prepared from nano-Pd colloid by surface adsorption process. Undoubtedly, the $Pd/Ce_{0.5}Zr_{0.5}O_2$-M3 exhibited also low Pd loading (0.27 wt%). For M1 and M2 samples (both Al_2O_3 and $Ce_{0.5}Zr_{0.5}O_2$), the actual Pd contents were higher than the corresponding samples prepared by the M3 process, indicating that the M1 and M2 processes benefited to the loading of Pd nanoparticles on the surface of Al_2O_3 and $Ce_{0.5}Zr_{0.5}O_2$. The metal dispersion determined by H_2–O_2 titration was in similar level for all catalysts, except for the Pd/Al_2O_3-M3 (5.3%) and $Pd/Ce_{0.5}Zr_{0.5}O_2$-M1 (7.9%) samples.

The H_2-TPR profiles of Pd/Al_2O_3 and $Pd/Ce_{0.5}Zr_{0.5}O_2$ catalysts were shown in Fig. 6. An obvious negative peak at ca. 70 °C appeared

Table 3
Physico-chemical properties of Pd/Al_2O_3 and $Pd/Ce_{0.5}Zr_{0.5}O_2$ catalysts.

Catalyst	BET surface area (m^2/g)	Pore volume (cm^3/g)	Pore size (nm)	Actual Pd (wt%)	Metal dispersion (%)
Pd/Al_2O_3-M1	302.2	0.39	4.0	0.96	41.9
Pd/Al_2O_3-M2	280.4	0.35	4.0	1.00	53.4
Pd/Al_2O_3-M3	233.2	0.38	5.1	0.44	5.3
$Pd/Ce_{0.5}Zr_{0.5}O_2$-M1	67.8	0.072	3.7	0.77	7.9
$Pd/Ce_{0.5}Zr_{0.5}O_2$-M2	40.7	0.046	3.8	0.75	39.3
$Pd/Ce_{0.5}Zr_{0.5}O_2$-M3	35.5	0.059	4.5	0.27	36.7

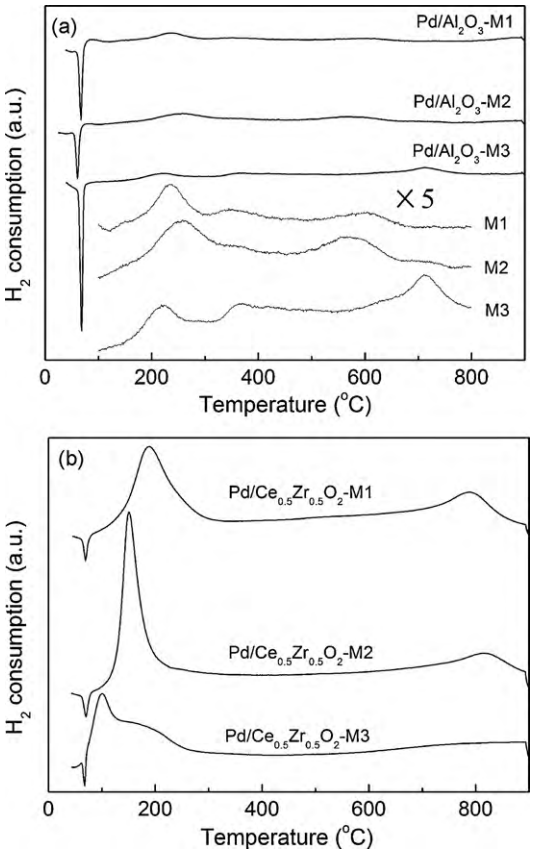

Fig. 6. H_2-TPR profiles of Pd/Al_2O_3 (a) and $Pd/Ce_{0.5}Zr_{0.5}O_2$ (b) catalyst.

for all catalysts investigated, indicating the hydrogen releasing during the TPR procedure that might be due to the decomposition of palladium hydride (β-PdH_x) [24]. The dispersed PdO species can be reduced at subambient temperature (even below 0 °C) [24,27]. Therefore, it is not possible to observe this PdO reduction peak because our TPR experiment started from about 35 °C. At the same time, some hydrogen molecules could dissociate and form PdH_x species by interacting with Pd [24] or PdO [26] on catalyst surface. The PdH_x species was unstable and decomposed to release molecular hydrogen at 70–100 °C [27]. The process can be expressed as follows:

$$PdO + H_2 \rightarrow Pd + H_2O \quad (2)$$

$$H_2 \rightarrow 2H \quad (3)$$

$$xH + Pd \rightarrow \beta\text{-}PdH_x \quad (4)$$

$$\beta\text{-}PdH_x \rightarrow Pd + 0.5xH_2 \quad (5)$$

The amounts of released H_2 calculated based on the negative peaks over the Al_2O_3 and $Ce_{0.5}Zr_{0.5}O_2$ supported catalysts were listed in Table 4. Due to the complexity of above process, the comparison of H_2 release was difficult. For example, the exact value of x in β-PdH_x was unknown and difficult to be estimated. However, the amounts of H_2 released from different catalysts, including both of Pd/Al_2O_3 and $Pd/Ce_{0.5}Zr_{0.5}O_2$, were in the level from 24 to 79 μmol/g.

The TPR curves above 100 °C were magnified fivefold for Pd/Al_2O_3 catalysts in Fig. 6a. One H_2 consumption peak at 200–300 °C appeared for the three samples, which corresponded to the reduction of PdO interacted strongly with alumina surface [27]. The other weak PdO reduction peak could be observed at 350–450 °C for Pd/Al_2O_3 samples, suggesting more intensive interaction occurred between PdO and alumina [22,24,28]. The peaks at higher temperature 500–650 °C (even 800 °C for Pd/Al_2O_3-M3) were ambiguous, which probably related to the rearrangement of the hydroxylated structure on Al_2O_3 support [29]. The theoretical amounts of H_2 consumed on reduction of PdO over the Pd/Al_2O_3-M1, Pd/Al_2O_3-M2, and Pd/Al_2O_3-M3 samples were 90, 94, and 42 μmol/g, respectively, which were generally higher than the values obtained in TPR data processing (Table 4), approving the partial reduction of PdO species at low temperature. As stated above, the quantitative relation between H_2 consumption and release was hard to be evaluated because the composition of palladium hydride (β-PdH_x) was unclear.

Compared to the Pd/Al_2O_3 sample, the bigger reduction peaks were observed over the $Pd/Ce_{0.5}Zr_{0.5}O_2$ (-M1, -M2, and -M3) catalysts at 100–300 °C and another peak appeared at ca. 800 °C for $Pd/Ce_{0.5}Zr_{0.5}O_2$-M1 and $Pd/Ce_{0.5}Zr_{0.5}O_2$-M2 samples. The amounts of H_2 consumption based on the reduction peaks were calculated and presented in Table 4. It can be seen that the values were in the range of 1165–1476 μmol/g and much higher than theoretical amounts consumed by PdO reduction, which were 73, 71 and 26 μmol/g for $Pd/Ce_{0.5}Zr_{0.5}O_2$-M1, $Pd/Ce_{0.5}Zr_{0.5}O_2$-M2 and $Pd/Ce_{0.5}Zr_{0.5}O_2$-M3, respectively. It was obvious that these peaks were not completely contributed by the reduction of PdO species. It was reported that the reduction peaks at low temperature over $Pd/Ce_{0.5}Zr_{0.5}O_2$ should be assigned to the reduction of both PdO species and Ce^{4+} in $Ce_{0.5}Zr_{0.5}O_2$ solid solution [30]. The high temperature reduction at 800 °C for $Pd/Ce_{0.5}Zr_{0.5}O_2$-M1 and $Pd/Ce_{0.5}Zr_{0.5}O_2$-M2 could be assigned to the reduction of lattice oxygen in $Ce_{0.5}Zr_{0.5}O_2$ [24]. Stoichiometrically, 1 g $Ce_{0.5}Zr_{0.5}O_2$ required 1700 μmol/g H_2 for a complete reduction of Ce^{4+} to Ce^{3+}. The quantity of $Ce^{4+} \rightarrow Ce^{3+}$ reduction was in the order of $Ce_{0.5}Zr_{0.5}O_2$-M2(1476) > $Ce_{0.5}Zr_{0.5}O_2$-M1(1363) > $Ce_{0.5}Zr_{0.5}O_2$-M3(1165). While the reduction temperature was in the sequence of $Ce_{0.5}Zr_{0.5}O_2$-M1(188 °C) > $Ce_{0.5}Zr_{0.5}O_2$-M2 (150 °C) > $Ce_{0.5}Zr_{0.5}O_2$-M3 (100 °C) (Fig. 6b). The partial reduction of CeO_2 at low temperature (100–200 °C) was also observed by Wang et al. when they did research on Pd/CeO_2 catalyst for CO oxidation [30]. The reduction at low temperature may associate with the hydrogen spillover from the metal to the support and metal–support strong interaction [24], which would promote the reduction of Ce^{4+} ions.

At last, the catalytic activities of all Pd/Al_2O_3 and $Pd/Ce_{0.5}Zr_{0.5}O_2$ catalysts for CO oxidation were investigated and the results were summarized in Fig. 7. For Pd/Al_2O_3 catalysts, the activity was increased in the order of Pd/Al_2O_3-M1 (190 °C) < Pd/Al_2O_3-M2 (200 °C) < Pd/Al_2O_3-M3 (230 °C) samples, suggesting that the process of Al_2O_3 preparation in Pd colloid was benefit to the enhancement in catalytic CO oxidation activity of Pd/Al_2O_3 cat-

Table 4
The H_2 release and consumption in H_2-TPR process over Pd/Al_2O_3 and $Pd/Ce_{0.5}Zr_{0.5}O_2$ catalysts (μmol/g).

Samples	Pd/Al_2O_3			$Pd/Ce_{0.5}Zr_{0.5}O_2$		
	M1	M2	M3	M1	M2	M3
H_2 release (negative peak)	36	26	79	50	55	24
H_2 consumption (positive peak)	72	68	40	1363	1476	1165

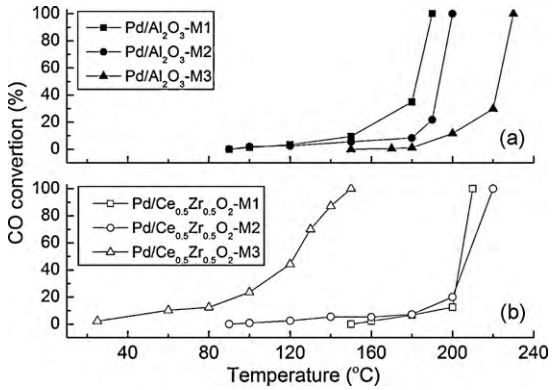

Fig. 7. CO oxidation activity over Pd/Al_2O_3 (a) and $Pd/Ce_{0.5}Zr_{0.5}O_2$ (b) catalysts. Reaction conditions: 1% CO, 1% O_2, He balance; catalyst weight = 0.05 g, SV = 60,000 h^{-1}.

alyst. The low actual Pd loading may be responsible for the low activity due to the reduction of active components for these Pd/Al_2O_3 catalysts. However, the CO oxidation activities over the three $Pd/Ce_{0.5}Zr_{0.5}O_2$ catalysts were absolutely different. The $Pd/Ce_{0.5}Zr_{0.5}O_2$-M3 catalyst showed the highest activity, namely, the lowest CO total conversion temperature in the three samples.

As above statement, the catalytic activity of supported Pd-based catalysts was dominated by many factors, such as the number of exposed Pd particles, the reducibility of PdO_x species, and the surface structure. The number of exposed Pd particles on catalyst surface has been discussed in previous text, which can be still applied for elucidation of activities on Pd/Al_2O_3 samples. The Pd/Al_2O_3-M3 showed lower activity than other two Pd/Al_2O_3 samples in CO oxidation (Fig. 7) due to the small quantity of exposed Pd species over the Pd/Al_2O_3-M3 catalyst (0.02×10^{-4} g/g for Pd/Al_2O_3-M3, 0.4×10^{-4} for Pd/Al_2O_3-M1, and 0.53×10^{-4} for Pd/Al_2O_3-M2), which was calculated by multiplying of actual Pd content and metal dispersion. However, the number of exposed Pd atoms was not only factor to govern the catalytic activity of $Pd/Ce_{0.5}Zr_{0.5}O_2$ sample. The $Pd/Ce_{0.5}Zr_{0.5}O_2$-M3 with the highest activity exhibited just a medium exposed Pd atoms value of 0.1×10^{-4} g/g. Whereas the numbers of exposed Pd atoms for $Pd/Ce_{0.5}Zr_{0.5}O_2$-M1 and $Pd/Ce_{0.5}Zr_{0.5}O_2$-M2 were 0.06×10^{-4} and 0.29×10^{-4} g/g, respectively.

The reducibility of Pd species was also an important factor to influence the activity. However, in the TPR process of $Pd/Ce_{0.5}Zr_{0.5}O_2$ samples, the reduction of PdO and Ce^{4+} ions partial reduction occurred simultaneously. Since the Ce^{4+} can be reduced at temperature as low as 100–200 °C, they could participate in the reaction through redox cycle. It was particularly true under the real TWC reaction process. The easily reduced CeO_2 and PdO species at low temperature were found on $Pd/Ce_{0.5}Zr_{0.5}O_2$-M3 sample (TPR results), which were crucial for participation of Ce^{4+}/Ce^{3+} and PdO/Pd species in the redox cycle in CO oxidation. The cycle of Ce^{4+}/Ce^{3+} at low temperature less than 200 °C may be very important, since it was not observed in Pd/CeO_2 sample (not plotted here). So the Pd/CeO_2 exhibited lower activity than $Pd/Ce_{0.5}Zr_{0.5}O_2$ in spite of its higher metal dispersion. Similarly, the lower reducibility of PdO particles would decrease the catalytic activity of Pd/Al_2O_3 catalyst, which had also been observed by Groppi [31]. The Ce^{4+} species that can be reduced at high temperature (~800 °C) should have not significant contribution on the activity of $Pd/Ce_{0.5}Zr_{0.5}O_2$ catalysts, because the CO was totally converted below 250 °C. The reducibility of PdO species also may be accounted for the activity difference of Pd/Al_2O_3-M1 and Pd/Al_2O_3-M2 catalysts. Although Pd/Al_2O_3-M1 catalyst possessed a lower number of exposed Pd atoms (0.4×10^{-4}) than Pd/Al_2O_3-M2 (0.53×10^{-4}), a little higher activity was gotten on Pd/Al_2O_3-M1 catalyst. The reduction of PdO species appeared on Pd/Al_2O_3-M1 happened at ca. 230 °C, which was lower than that on Pd/Al_2O_3-M2 (260 °C).

4. Conclusions

The ultrasonic-assisted membrane reduction (UAMR) method was successfully applied for assembly of colloidal Pd nanocrystals. The Pd particle size could be controlled in the range of several to several hundreds nanometers by regulating synthesis parameters in UAMR process. The supported Pd catalysts were prepared from the nano-Pd colloid fabricated by UAMR. The support property had significant influence on the actual Pd loading and CO oxidation activity of as-prepared catalysts when the Pd nanoparticles were loaded by adsorbing on support surface. The preparation of support (Al_2O_3 and $Ce_{0.5}Zr_{0.5}O_2$) in the Pd colloid could produce catalyst with large surface area and pore volume. Both the number of exposed Pd species and reducibility of PdO_x on the catalyst dominated the catalytic activity.

Acknowledgements

The authors are grateful for the financial support of the projects by the National Natural Science Foundation of China (granting No. 20877006, 20833011), National 863 Program Foundation of China (granting No. 2009AA063201) and Beijing Municipal Science & Technology Commission (granting No. 2101002).

References

[1] H.S. Gandhi, G.W. Graham, R.W. McCabe, J. Catal. 216 (2003) 433.
[2] M. Shelef, R.W. McCabe, Catal. Today 62 (2000) 35.
[3] S. Matsumoto, Catal. Today 90 (2004) 183.
[4] H. Birgersson, M. Boutonnet, F. Klingstedt, D.Y. Murzin, P. Stefanov, A. Naydenov, Appl. Catal. B 65 (2006) 93.
[5] M. Fernández-García, A. Iglesias-Juez, A. Martínez-Arias, A.B. Hungría, J.A. Anderson, J.C. Conesa, J. Soria, J. Catal. 221 (2004) 594.
[6] A.B. Gaspar, L.C. Dieguez, Appl. Catal. A 201 (2000) 241.
[7] M.S. Chen, D.W. Goodman, Chem. Soc. Rev. 37 (2008) 1860.
[8] R.M. Rioux, B.B. Hsu, M.E. Grass, H. Song, G.A. Somorjai, Catal. Lett. 126 (2008) 10.
[9] G.A. Somorjai, J.Y. Park, Chem. Soc. Rev. 37 (2008) 2155.
[10] S. Zhou, B. Varughese, B. Eichhorn, G. Jackson, K. McIlwrath, Angew. Chem. Int. Ed. 44 (2005) 4539.
[11] G. Agostini, R. Pellegrini, G. Leofanti, L. Bertinetti, S. Bertarione, E. Groppo, A. Zecchina, C. Lamberti, J. Phys. Chem. C 113 (2009) 10485.
[12] B.L. Cushing, V.L. Kolesnichenko, C.J. O'Connor, Chem. Rev. 104 (2004) 3893.
[13] Y. Xia, Y. Xiong, B. Lim, S.E. Skrabalak, Angew. Chem. Int. Ed. 48 (2009) 60.
[14] R. Narayanan, M.A. El-Sayed, J. Phys. Chem. B 109 (2005) 12663.
[15] S. Alayoglu, A.U. Nilekar, M. Mavrikakis, B. Eichhorn, Nat. Mater. 7 (2008) 333.
[16] L.C. Liu, T. Wei, X. Guan, X.H. Zi, H. He, H.X. Dai, J. Phys. Chem. C 113 (2009) 8595.
[17] D. Lu, K.J. Tanaka, J. Phys. Chem. B 101 (1997) 4030.
[18] M.F. Luo, Z.Y. Hou, X.X. Yuan, X.M. Zheng, Catal. Lett. 50 (1998) 205.
[19] S.M. McClure, D.W. Goodman, Chem. Phys. Lett. 469 (2009) 1.

[20] W. Lin, Y.X. Zhu, N.Z. Wu, Y.C. Xie, I. Murwani, E. Kemnitz, Appl. Catal. B 50 (2004) 59.
[21] V. Ferrer, A. Moronta, J. Sánchez, R. Solano, S. Bernal, D. Finol, Catal. Today 107–108 (2005) 487.
[22] J. Vinod Kumar, N. Lingaiah, K.S. Rama Rao, S.P. Ramnani, S. Sabharwal, P.S. Sai Prasad, Catal. Commun. 10 (2009) 1149.
[23] B. Yue, R. Zhou, Y. Wang, X. Zheng, J. Mol. Catal. A 238 (2005) 241.
[24] L.F. Chen, G. González, J.A. Wang, L.E. Noreña, A. Toledo, S. Castillo, M. Morán-Pineda, Appl. Surf. Sci. 243 (2005) 319.
[25] Z. Zhou, S. Ji, F. Yin, Z. Lu, C. Li, J. Fuel Chem. Technol. 35 (2007) 583.
[26] C.-B. Wang, H.-K. Lin, C.-M. Ho, J. Mol. Catal. A 180 (2002) 285.
[27] F. Pinna, F. Menegazzo, M. Signoretto, P. Canton, G. Fagherazzi, N. Pernicone, Appl. Catal. A 219 (2001) 195.
[28] M. Cobo, A. Quintero, C.M. Correa, Catal. Today 133–135 (2008) 509.
[29] A. Barrera, M. Viniegra, P. Bosch, V.H. Lara, S. Fuentes, Appl. Catal. B 34 (2001) 97.
[30] H. Zhu, Z. Qin, W. Shan, W. Shen, J. Wang, J. Catal. 225 (2004) 267.
[31] P. Castellazzi, G. Groppi, P. Forzatti, A. Baylet, P. Marécot, D. Duprez, Catal. Today (2009), doi:10.1016/j.cattod.2009.02.029.